Decentralized Geolocation and Optimal Path Planning Using Limited UAVs

Sean R. Semper
Graduate Student
srsemper@buffalo.edu

John L. Crassidis
Professor
johnc@buffalo.edu

Department of Mechanical & Aerospace Engineering
University at Buffalo, State University of New York, Amherst, NY 14260–4400

Abstract – *A decentralized estimation architecture for determining an object's absolute position from relative position measurements, commonly called geolocation, is developed in this paper. Relative measurements are obtained from a two unmanned aerial vehicle (UAV) team with electronic support measure (ESM) sensors on board. One team combines their time of arrival (TOA) measurements forming one time difference of arrival measurement (TDOA) from an emitter's signal. Using an Extended Kalman Filter (EKF), pseudorange equations containing UAV positions and emitter position estimates are sequentially estimated to solve for absolute emitter positions. When N UAV teams are available, a decentralized EKF architecture is derived to optimally fuse estimates from N filters at the global fusion node. In addition, optimal trajectories for two UAVs are developed to minimize the covariance position errors. Weights are placed on the UAV motions, so minimum and maximum distances to the emitting object are restricted.*

Keywords: decentralized geolocation, TDOA, estimation, optimal control

1 Introduction

Geolocation has grown in popularity presently due to the multi-disciplinary engineering topics it involves and the need to efficiently locate friendly or hostile emitting sources. Geolocation by TDOA consist primarily of distress or hostile signals which may or may not cause electronic interference [1–3]. Previous methods to estimate these source locations relied on batch processing or rigorous analytical solutions [1, 4–7]. Those methods obviously require a number of sensors greater than the number of unknown position state estimates. Recently [8–10] implemented recursive estimation to solve the TDOA geolocation problem with the EKF, Unsented Kalman Filter (UKF) and a hybrid in conjunction with a Gaussian sum approximation. Specifically, [9–11] applied measurement association and showed the two sensor case where location unknowns are equal to the number of sensors, solutions are then recursively updated. From this foundation using 2 UAVs to N UAVs and $N/2$ UAV teams, a decentralized estimation architecture for geolocation of emitters is derived here.

Because geolocation is implemented in a centralized architecture it has the simplest approach (time correlation) and is very useful to compare the decentralized architecture performance. A centralized architecture has $N-1$ UAVs as the sensors and the N^{th} UAV as the only filter. This works well for a straightforward implementation, but has severe disadvantages regardless of hostile or friendly environments. If the master UAV (central filter) is lost due to terrain, hostile actions, poor maintenance, etc., all geolocation processing halts. Uploading filter software or pulling a UAV out of a distant mission to physically upload software is unreasonable, due to the evasiveness of a target and mission cost. In addition, central processing requires the system engineer to consider communication bandwidth and available processing to produce a single estimate [12]. There is always a tradeoff between bandwidth and processing power in order to meet general system requirements. Using a decentralized approach for geolocation we can avoid various failures, distribute filtering tasks then add robustness to the overall system architecture [13, 14]. Also we can focus on individual UAV team control efforts and still achieve optimal estimates.

From the TDOA measurement equation, it is known that filter performance is a function of the emitter position and individual UAV positions. Characteristics for performance are noted by minimal (or maximum) time to convergence and tolerable error bounds. Since the emitter's position is unknown the performance depends heavily on the UAV motion. With no UAV motion the emitter becomes unobservable, especially when limiting the number of UAVs performing a geolocation task. Most UAVs fly pre-programmed flight paths and are allowed limited flight path changes via ground station controllers. However, ground station controllers are not ideally suited for guiding UAVs to optimize geolocation performance [15]. Implementing optimal control techniques allows for compromise between preprogrammed flight and the anticipated optimal guidance.

The paper is organized in the following manner, Section 2 introduces the fundamental TDOA geolocation, a hyperbolic method which uses time differences of arrivals of radio emissions. Section 3 presents an EKF specifically for recursive geolocation estimation. Section 4 describes a decentralized/distributed fusion architectures for multiple UAV teams. Also within this section the Covariance Inter-

section algorithm used for information fusion in decentralized geolocation is shown. Section 5 uses optimal control techniques for minimizing error bounds on geolocation estimates through a velocity control scheme. Section 6 presents individual simulation results for Sections 4 and 5, which are decentralized geolocation and optimal paths for a single UAV team, respectively.

2 Limited Sensor TDOA Geolocation

When multiple sensors are not available, geolocating a position obviously becomes very difficult but not impossible. If at least two sensors are available then positioning them at multiple points in space to increase the observation of the object is required. Now, consider two UAVs at known location $X_k^i = (x_k^i, y_k^i)$ and both are equipped with electronic support measures (ESM) and GPS. These sensors are capable of intercepting discrete or signal transmissions from an emitting object. Also consider an object at location $x_k^e = (x_k, y_k)$ that emits an omni-directional signal at distinct time instant t_k. If this signal is intercepted by UAV i at time instant t_k we have

$$t_k^i = t_k + \frac{r_k^i}{c} \tag{1}$$

where r_k^i is the range from UAV i position to the emitting object, given by

$$r_k^i = \sqrt{(x_k - x_k^i)^2 + (y_k - y_k^i)^2} \tag{2}$$

and c the speed of propagation is 300,000 km/s for typical radio emissions.

Since the object's position and time of origin for the emitted signal are not known, Eq. (1) has more unknowns than equations to solve. However, we do know TOA's to each UAV because of the ESM observations. By choosing one UAV as the reference sensor a TDOA from ESM sensors 1 and 2 gives a modified equation

$$t_k^{i1} = t_k^i - t_k^1 = \frac{r_k^i - r_k^1}{c} \tag{3}$$

We can also relate the reference UAV-(1) to any other UAV-(i) if they become present and capable, by pairing N UAV measurements together where $i = 2, 3, \ldots N$.

3 Extended Kalman Filter for Geolocation

The unknown emitter is a continuous-time (constant velocity) differential truth model given by

$$\dot{\mathbf{x}}(t) = F\mathbf{x}(t) + G\mathbf{w}(t) \tag{4}$$

where $\mathbf{w}(t)$ is the process noise with covariance Q. In the filter Q will be used as a tuning parameter for improving state estimates. Since discrete time sampling is used the state transition matrix transformation gives

$$\Phi(t, t_0) = I + F\Delta t = \begin{bmatrix} 1 & \Delta t & 0 & 0 \\ 0 & 1 & 0 & 0 \\ 0 & 0 & 1 & \Delta t \\ 0 & 0 & 0 & 1 \end{bmatrix} \tag{5}$$

where $\Delta t = (t - t_0)$ is the sampling interval for both truth and measurement models. With $Q = q$, a scalar and $G = \begin{bmatrix} 0 & 1 & 0 & 1 \end{bmatrix}$ the discrete-time process noise covariance for model propagation becomes

$$\Upsilon Q \Upsilon^T = q \begin{bmatrix} \Delta^3 t/3 & \Delta^2/2 & 0 & 0 \\ \Delta^2 t/2 & \Delta t & 0 & 0 \\ 0 & 0 & \Delta^3 t/3 & \Delta^2 t/2 \\ 0 & 0 & \Delta^2 t/2 & \Delta t \end{bmatrix} \tag{6}$$

This results in the discrete time truth-model with the state-transition matrix

$$\mathbf{x}_{k+1} = \Phi_k \mathbf{x}_k + \Upsilon \mathbf{w}_k \tag{7}$$

where $\mathbf{w}_k$ has covariance Q_k. Note that for small Δt the approximation $\Upsilon Q \Upsilon^T = \Delta t G Q G$ can be used [16].

The measurement model comes from the TDOA equation in Section 2, considering two UAVs. Measurements for TDOAs are commonly converted to range difference of arrival (RDOA) by multiplying the TDOA with the speed of propagation c. This modified measurement is rewritten as

$$\tilde{y}_k = c(t_k^2 - t_k^1) = h_k(\mathbf{x}_k) + v_k \tag{8}$$

where

$$h_k(\mathbf{x}_k) = (r_k^2 - r_k^1) \tag{9}$$

and the range, r_k^i, is written the same as in Eq. (2). The sensor's measurement noise v_k is a zero-mean Gaussian white-noise process with variance given by σ_t^2. Since the measurement is in the form of range, the clock variance is multiplied by the speed of propagation squared, yielding $R_k = c^2\sigma_t^2$, where R_k is the measurement variance used for the EKF.

The sensitivity matrix, H, is a Jacobian matrix for the nonlinear measurement model equation, $h_k(\hat{\mathbf{x}}_k)$. In discrete time this function is evaluated at time t_k using the estimated state vector $\hat{\mathbf{x}}_k$, resulting in

$$H(\hat{\mathbf{x}}_k^-) = \left.\frac{\partial \mathbf{h}}{\partial \mathbf{x}}\right|_{\hat{\mathbf{x}}^-} = \begin{bmatrix} \frac{\partial \mathbf{h}}{\partial x} & \frac{\partial \mathbf{h}}{\partial \dot{x}} & \frac{\partial \mathbf{h}}{\partial y} & \frac{\partial \mathbf{h}}{\partial \dot{y}} \end{bmatrix} \tag{10a}$$

$$= \begin{bmatrix} h_{11} & \ldots & h_{14} \end{bmatrix} \tag{10b}$$

Of the four emitter states, only two position states appear in the measurement function, thus partial velocities terms are

$$h_{12} = h_{14} = \frac{\partial \mathbf{h}}{\partial \dot{x}} = \frac{\partial \mathbf{h}}{\partial \dot{y}} = 0 \tag{11a}$$

Solving all partial derivatives gives

$$\frac{\partial \mathbf{h}}{\partial x} = h_{11} = \left(\frac{\hat{x}_k^- - x_k^2}{\hat{r}_k^2} - \frac{\hat{x}_k^- - x_k^1}{\hat{r}_k^1} \right) \quad (11b)$$

$$\frac{\partial \mathbf{h}}{\partial y} = h_{13} = \left(\frac{\hat{y}_k^- - y_k^2}{\hat{r}_k^2} - \frac{\hat{y}_k^- - y_k^1}{\hat{r}_k^1} \right) \quad (11c)$$

with

$$\hat{r}_k^i = \sqrt{(\hat{x}_k^- - x_k^i)^2 + (\hat{y}_k^- - y_k^i)^2} \quad (12)$$

This variable $\hat{r}_k^i$ corresponds to the estimated emitter range, unlike r_k^i which is used to generate simulated measurements with the true position for the EKF. Moreover we define $\hat{y}_k$ as the estimated RDOA:

$$\hat{y}_k = h(\hat{\mathbf{x}}_k^-) = (\hat{r}_k^2 - \hat{r}_k^1) \quad (13)$$

to reduce any confusion in the EKF formulation. The EKF equations are given by

$$K_k = P_k^- H_k^T [H_k P_k^- H_k^T + R_k]^{-1} \quad (14a)$$

$$\hat{\mathbf{x}}_k^+ = \hat{\mathbf{x}}_k^- + K_k(\tilde{\mathbf{y}}_k - \hat{\mathbf{y}}_k) \quad (14b)$$

$$P_k^+ = (I - K_k H_k) P_k^- \quad (14c)$$

$$\hat{\mathbf{x}}_{k+1}^- = \Phi_k \hat{\mathbf{x}}_k^+ \quad (14d)$$

$$P_{k+1}^- = \Phi_k P_k^+ \Phi_k^T + \Upsilon_k Q_k \Upsilon_k^T \quad (14e)$$

Referring to above, the EKF is invoked first with initial values for our state and covariance, $\hat{\mathbf{x}}_0^- = \hat{\mathbf{x}}_0$ and $P_0^- = P_0$. Then if a measurement is available, the state and covariance are updated by Eqs. (14a)-(14c), the Kalman gain and Kalman update equations, respectively, to $\hat{\mathbf{x}}_k^+$ and P_k^+. Next the propagation Eqs. (14d) and (14e) are used to carry the estimate and covariance to the next time-step, $\hat{\mathbf{x}}_{k+1}^+$ and P_{k+1}^+. However if a measurement is not available then the estimated state and covariance could be propagated until another measurement is received. This EKF provides the first local-node component for a decentralized architecture. In the next section the required global node and overall scheme are presented.

4 Decentralized Geolocation by Covariance Intersection

By designating a minimum of 2 UAVs as one team, their sensor measurement (input) and state estimate and error covariance (output) create one Local-EKF (LKF). Both UAVs contain sensors but only one UAV runs the "local-master EKF," thus locally we incorporate a centralized architecture. This team now sends its output to any base of operations where a Global-KF or Fusion Node (FN) processes incoming information. With N teams available the FN now takes all team outputs and fuses the estimate and error covariance from each LFK.

4.1 Fusion Architecture Requirements

For decentralized geolocation two main requirements are outlined within this section. The first is the number of teams including team members and secondly the communication constraints.

1. *Number of Teams & Members:* UAV teams must contain a minimum of 2 two UAVs and a maximum of N when implementing TDOA methods for geolocation. The upper limit is based on overall system performance and UAV availability. Increasing the number of teams reduces other points of failure for this decentralized architecture. Conversely, limiting team members reduces the need for a high workload on a single LKF and distributes the workload on LKF teams.

2. *Low Communication Bandwidth:* System performance is further increased by forcing low communication to each node, globally or locally. Low communication requirements are met by implementing a no feedback constraint to UAV teams. Directing communications in a single direction is applied in the hierarchical architecture.

The above requirements handles the minimum UAV case and N case senerio, providing the previously mentioned robustness for geolocation systems. At the FN the Covariance Intersection (CI) algorithm is implemented since it fulfills requirements 1 and 2.

4.2 Covariance Intersection

This section summarizes the CI algorithm [17] which is used to fuse redundant TOA information to produce consistent estimates regardless of the actual correlations. Consider *A* and *B*, two pieces of information which are fused together to yield an output *C*. Due to the sensors we know that *A* and *B* are corrupted by noise and as a result are random variables represented by their respective means **a** and **b**. Also we assume that the true statistics of these random variables are unknown but estimates of their statistics are available. The estimates of their means and covariances, $\{\mathbf{a}, P_{aa}\}$ and $\{\mathbf{b}, P_{bb}\}$ are taken from the node outputs within the decentralized architecture. True estimation errors are defined as $\tilde{\mathbf{a}} \equiv \mathbf{a} - \bar{\mathbf{a}}$ and $\tilde{\mathbf{b}} \equiv \mathbf{b} - \bar{\mathbf{b}}$, and the true covariance and cross-correlation are

$$\bar{P}_{aa} = E\{\tilde{\mathbf{a}}\tilde{\mathbf{a}}^T\}, \quad \bar{P}_{bb} = E\{\tilde{\mathbf{b}}\tilde{\mathbf{b}}^T\},$$

$$\bar{P}_{ab} = E\{\tilde{\mathbf{a}}\tilde{\mathbf{b}}^T\} \quad (15)$$

where the adorned symbols with a bar "$-$" denote the truth. Even if the true values of $\bar{P}_{aa}$ and $\bar{P}_{bb}$ are not known the only requirement is that

$$P_{aa} - \bar{P}_{aa} \geq 0 \quad \text{and} \quad P_{bb} - \bar{P}_{bb} \geq 0 \quad (16)$$

which assumes the estimates for **a** and **b** are consistent. By assuring consistency, the covariance must be equal or

greater than the true covariance. For the geolocation problem studied here, local estimates may be provided by, for example UAV-1 and 2 (Team 1) and UAV-3 and 2 (Team 2) where UAV-2 provides redundant information. Naively combining these separate estimates, may result in an inconsistent estimate.

4.2.1 Covariance Intersection Algorithm

The CI algorithm takes a convex combination of the estimate means and covariances in the information space, P^{-1}. This algorithm also exploits the *geometric* interpretation of the Kalman filter equations [17]. From this interpretation, we have the following approach: if P_{cc} is within the intersection of P_{aa} and P_{bb} for any possible choice of P_{ab}, then an update strategy that finds a P_{cc} which encloses the intersection region must be consistent even if there is no knowledge about P_{ab}. If P_{cc} encompasses the intersected information space very closely then the updated covariance uses the greatest amount of information from the convex combination [17, 18], which motivates the CI algorithm:

$$P_{cc}^{-1} = \omega P_{aa}^{-1} + (1-\omega)P_{bb}^{-1} \tag{17a}$$

$$P_{cc}^{-1}\mathbf{c} = \omega P_{aa}^{-1}\mathbf{a} + (1-\omega)P_{bb}^{-1}\mathbf{b} \tag{17b}$$

where $\omega \in [0,1]$ is a tuning parameter.

In the CI algorithm, the tuning parameter, ω, usually is chosen to minimize the trace of the covariance or the determinant of P_{cc}. By selecting cost functions which are convex with respect to ω, standard optimization tools can be used to find the global optimum. With $\sum_{i=1}^{n}\omega_i = 1$, this method is easily extended to the decentralized N UAV case by

$$P_{cc}^{-1} = \omega_1 P_{a_1a_1}^{-1} + \ldots + \omega_N P_{a_Na_N}^{-1} \tag{18a}$$

$$P_{cc}^{-1}\mathbf{c} = \omega_1 P_{a_1a_1}^{-1}\mathbf{a}_1 + \ldots + \omega_N P_{a_Na_N}^{-1}\mathbf{a}_N \tag{18b}$$

5 Optimal Guidance for Geolocation

Individual LKF performance is enhanced through a guidance routine where its primary goal is to improve state estimates and lower estimate errors. As mentioned before filter performance depends on emitter and UAV positioning which change over time. Section 2 and 3 discussed the TDOA problem and recursive filter solution which provided a clear example for where to look to improve our filter performance. By investigating the error covariance update equation a specific performance index is minimized that will provide a lower error covariance.

A common location fix, *rho-rho* ($\rho-\rho$) allows the use of standard definitions with Dilution of Precision (DOP) quantities for an indication "good" or "bad" geometries for a geolocation fix [3, 19]. DOP is a function of the error covariance matrix:

$$P = (H^T R^{-1} H)^{-1} \tag{19}$$

where H comes from Eqs. (10a)-(12) and R is the measurement variance. Also, defining the matrix $A \equiv (H^T H)^{-1}$ allows for the definition of other DOP quantities. The DOP quantity used is the position DOP (PDOP) which is given by

$$\text{PDOP} \equiv \sqrt{A_{11} + A_{22} + A_{33}} \tag{20}$$

When the geometry of the sensors is poor the estimate on the emitter location may have a low level of confidence and a high level of error (or diluted). Obtaining large values for A_{ii} are favorable since it reduces the error associated with an estimate. Considering the hyperbolic fix which arises from TDOA calculations we note that a larger difference between TOAs also increases the A matrix values. The simplest way to increase a TDOA is by positioning one UAV far from the estimated location and the second UAV closer to the estimated location.

As a result of the previous investigation the PDOP is selected to minimize our error covariance matrix through a modified Kalman updated equation given by

$$\mathcal{P}_k^+ = \mathcal{P}_k^- + H_k^T R_k^{-1} H_k \tag{21}$$

where the information matrix is $\mathcal{P} \equiv P^{-1}$. To minimize P_k^+ specifically, then $H_k^T R_k^{-1} H_k$ must be maximized as we noted before, $\mathcal{P}_k^-$ is a priori information. Previously we saw the PDOP defined in Eq. (20), however we can rewrite it as

$$\text{PDOP} \equiv \left\{ \text{Tr}\left[(H_k^T R_k^{-1} H_k) \right]^{-1} \right\}^{1/2} \tag{22}$$

Now the focus will be on minimizing one element of the error covariance, specifically the h_{11} element from Eq. (11b). Assuming the Y-locations of the UAVs are pre-selected, then omitting Z-locations for simplicity results in the determination of the optimal X-trajectories. In addition the control inputs to the system will be weighted to reduce unnecessary UAV motions. The following section formally introduces the full performance index.

5.1 Formal Problem Statement

To improve local filter performance we pose the following cost function:

$$\min \quad J[\mathbf{x}(t), \mathbf{u}(t), t] = \int_0^{t_f} \phi(\mathbf{x}(t), \mathbf{u}(t), t)dt \tag{23}$$

with

$$\mathbf{u}(t) \equiv \begin{bmatrix} u_1(t) & u_2(t) \end{bmatrix} \tag{24}$$

and

$$\begin{aligned} \phi \quad = \quad & -\left[\frac{\hat{x}(t) - x^{(2)}(t)}{\hat{r}^{(2)}(t)} - \frac{\hat{x}(t) - x^{(1)}(t)}{\hat{r}^{(1)}(t)} \right]^2 \\ & + w_1[u_1(t)]^2 + w_2[u_2(t)]^2 \end{aligned} \tag{25}$$

subject to:

$$\text{State Inputs:} \begin{cases} \dot{x}^{(1)}(t) = u_1(t) \\ \dot{x}^{(2)}(t) = u_2(t) \end{cases} \tag{26}$$

where w_1 and w_2 are weights on the square of the velocity control input and $u_1(t)$ and $u_2(t)$ are velocity control inputs. Squaring $u_i(t)$ corresponds to the expended power/energy of the overall UAV system.

5.2 Velocity Control

From optimal control theory [20], the Hamiltonian is constructed with the following change of variables, $s_i \equiv x^{(i)}$ and $\hat{r}_i \equiv \hat{r}^{(i)}$:

$$\mathcal{H} = -\left[\frac{\hat{x}-s_2}{\hat{r}_2} - \frac{\hat{x}-s_1}{\hat{r}_1}\right]^2 + w_1[u_1]^2 + w_2[u_2]^2 + \lambda_1 u_1 + \lambda_2 u_2 \quad (27)$$

Euler-Lagrange equations partial derivatives, $\left(\frac{\partial \mathcal{H}}{\partial \mathbf{s}}\right) \equiv -\dot{\lambda}$ and $\left(\frac{\partial \mathcal{H}}{\partial \lambda}\right) = \begin{bmatrix} \dot{s}(1) & \dot{s}(2) \end{bmatrix}$ are given by,

$$-\dot{\lambda}_1 = 2\left(\frac{\hat{x}-s_2}{\hat{r}_2} - \frac{\hat{x}-s_1}{\hat{r}_1}\right)\left(\frac{1}{\hat{r}_1} - \frac{(\hat{x}-s_1)^2}{(\hat{r}_1)^3}\right) \quad (28)$$

$$-\dot{\lambda}_2 = 2\left(\frac{\hat{x}-s_2}{\hat{r}_2} - \frac{\hat{x}-s_1}{\hat{r}_1}\right)\left(\frac{1}{\hat{r}_2} - \frac{(\hat{x}-s_1)^2}{(\hat{r}_2)^3}\right) \quad (29)$$

Equations (28) and (29) are the co-state differential equations and the state differential equations are given by following:

$$\dot{s}_1 = u_1 \quad (30)$$

$$\dot{s}_2 = u_2 \quad (31)$$

Next we solve $\left(\frac{\partial \mathcal{H}}{\partial \mathbf{u}}\right) = 0$ so we can eliminate $\mathbf{u}_i(t)$ from Eqs. (30) and (31) which gives

$$\left(\frac{\partial \mathcal{H}}{\partial u_1}\right) = 2w_1 u_1 + \lambda_1 = 0 \quad (32)$$

$$\left(\frac{\partial \mathcal{H}}{\partial u_2}\right) = 2w_2 u_2 + \lambda_2 = 0 \quad (33)$$

Solving for the control vector $\mathbf{u}_i(t)$ components yields

$$u_1 = \frac{-\lambda_1}{2w_1} \quad (34)$$

$$u_2 = \frac{-\lambda_2}{2w_2} \quad (35)$$

Now substituting in Eqs. (34) and (35) and rewriting the state Eqs. (30) and (31) gives

$$\dot{s}_1 = \frac{-\lambda_1}{2w_1} \quad (36)$$

$$\dot{s}_2 = \frac{-\lambda_2}{2w_2} \quad (37)$$

Endpoint constraints values for states equations are selected from predetermined linear trajectories for both UAVs and co-states values are free. At t_0 we use

$$s_1(t_0) = [5000\text{ m}] \quad s_2(t_0) = [2900\text{ m}]$$
$$\lambda_1(t_0) = [\text{Free}] \quad \lambda_2(t_0) = [\text{Free}] \quad (38)$$

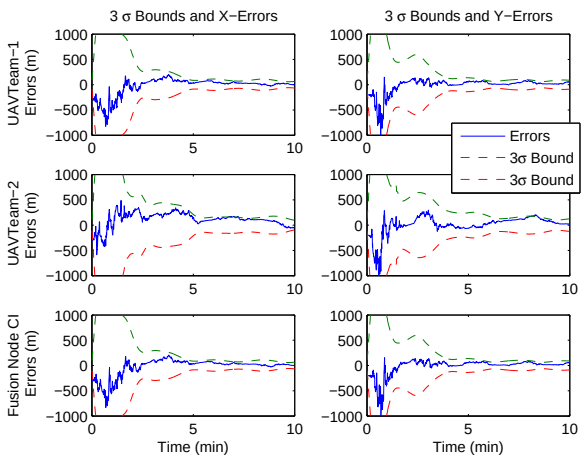

Figure 1: Simulation 1 Team-1, Team-2 and CI Comparison

and weights for the control input are

$$w_1 = 0.02 \quad \text{and} \quad w_2 = 0.01 \quad (39)$$

There are now four coupled differential equations (2 co-states and 2 states equations) which are solved using numerical integration.

6 Simulation Results

6.1 Covariance Intersection

Two simulations are performed using different measurement clock standard deviation values, $\sqrt{\sigma_t^2} = 1.0 \times 10^{-6}$ and 1.0×10^{-7} (sec). The initial state estimates are $\hat{\mathbf{x}}_0 = \begin{bmatrix} 0 & 0 & 0 & 0 \end{bmatrix}^T$ (m) and the true emitter position is $\mathbf{x}_0 = \begin{bmatrix} 300 & 0 & 200 & 0 \end{bmatrix}^T$(m). The simulation time duration is 10 minutes with a sampling time of $\Delta t = 0.6$ seconds. The trajectories for all three UAVs are fixed to elliptical shapes given by

$$\text{UAV}_1\text{:} \begin{bmatrix} x(t) \\ y(t) \end{bmatrix} = \begin{bmatrix} 1450\sin(t/50) \\ 2150\cos(t/50) \end{bmatrix} \text{(m)} \quad (40a)$$

$$\text{UAV}_2\text{:} \begin{bmatrix} x(t) \\ y(t) \end{bmatrix} = \begin{bmatrix} 2050\sin(t/40) \\ 1550\cos(t/40) \end{bmatrix} \text{(m)} \quad (40b)$$

$$\text{UAV}_3\text{:} \begin{bmatrix} x(t) \\ y(t) \end{bmatrix} = \begin{bmatrix} 4050\sin(t/45) \\ 2750\cos(t/45) \end{bmatrix} \text{(m)} \quad (40c)$$

The two teams contain the following members

$$\text{TEAM-1:} \left\{ \begin{array}{c} \text{UAV-1} \\ \text{UAV-2} \end{array} \right\} \text{ \& TEAM-2:} \left\{ \begin{array}{c} \text{UAV-1} \\ \text{UAV-3} \end{array} \right\}$$

Each team's 3σ error bounds are plotted together in Figure 1 revealing the overall geolocation accuracies, where Team-2 has an inferior accuracy. This results in the FN

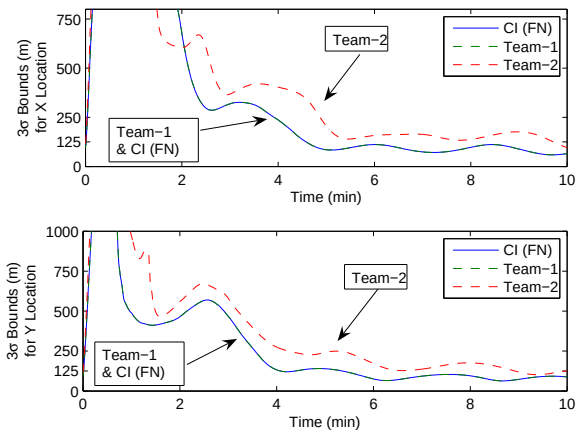

Figure 2: Simulation 1 Team-1 and Team-2 vs. CI Geolocation 3σ Bounds

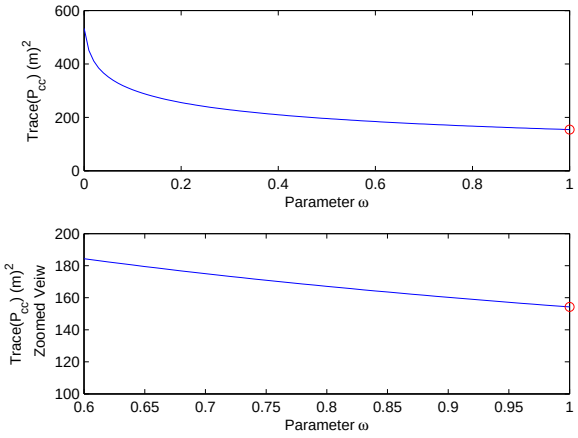

Figure 3: Simulation 1 $P_{cc}(\omega)$ vs. Parameter ω and Optimum

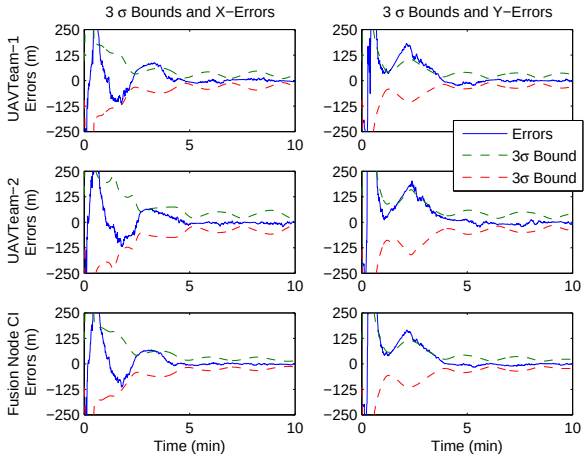

Figure 4: Simulation 2 Team-1, Team-2 and CI Comparison

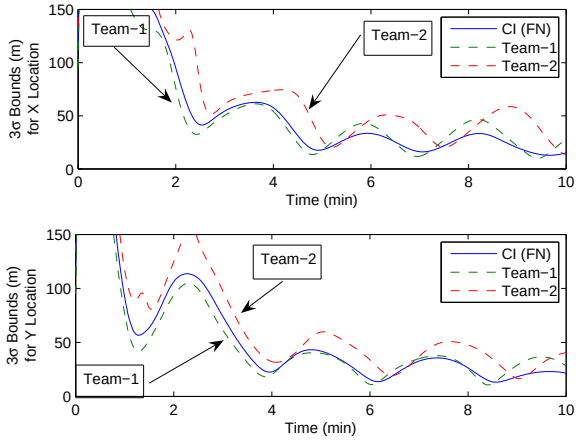

Figure 5: Simulation 2 Team-1 and Team-2 vs. CI Geolocation 3σ Bounds

completely weighting the Team-2 inputs as zero, $\omega_2 = 0$ and weighting Team-1 inputs as, $\omega_1 = 1$ (where $\omega \equiv \omega_1$ and $1 - \omega \equiv \omega_2$). This is visually confirmed in Figures 2 where Team-1 and the FN has identically positive x and y location error-bounds and Figure 3 where the optimum of $P_{cc}(\omega)$ is plotted with the optimal value of 1.

For simulation 2, node-to-node comparison seen in Figure 4 contains the familiar error bound convergence properties, with some error outside the bounds before the 4 minute mark. However at the FN the CI algorithm no longer eliminates Team-2 inputs but optimally weights Team-1 with $\omega_1 = 0.4014$ and Team-2 with $\omega_2 = 0.5986$ (see Figure 6). This comes from the fact that Team-2 error bounds still are larger, so that at the FN the CI algorithm fits the tightest P_{cc} ellipse possible around both P_{aa} (Team-1) and P_{bb} (Team-2) error ellipses. Figure 5 agrees with this explaination since the FN error bounds for half the portion of the simulation ($t \approx 5$ mins) are in between the Team-1 and 2 error bounds. Once the error bounds settle, the geolocation accuracy is within 50 meters for each position state estimate. The FN accuracy considered is from the maximum heights seen from the oscillating 3σ error bounds in Figure 5, not the minimal values.

6.2 Velocity Control Results

For this simulation, the first EKF is executed forward in time and the geolocation data, such as error covariance, 3σ error bounds geolocation state estimates and UAV trajectories, are stored for use in an optimal guidance routine. The truth cannot be used within the routine, only state estimates, since the emitter location is unknown. Then a second EKF with the same parameters, except for the replaced $\mathbf{x}(t)$ UAV path, is executed again forward in time to observe any improve-

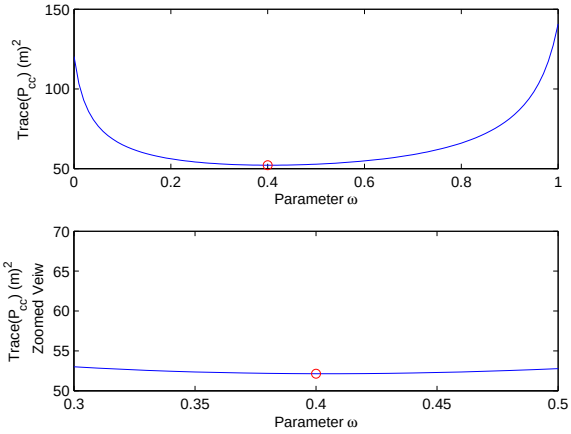

Figure 6: Simulation 2 $P_{cc}(\omega)$ vs. Parameter ω and Optimum

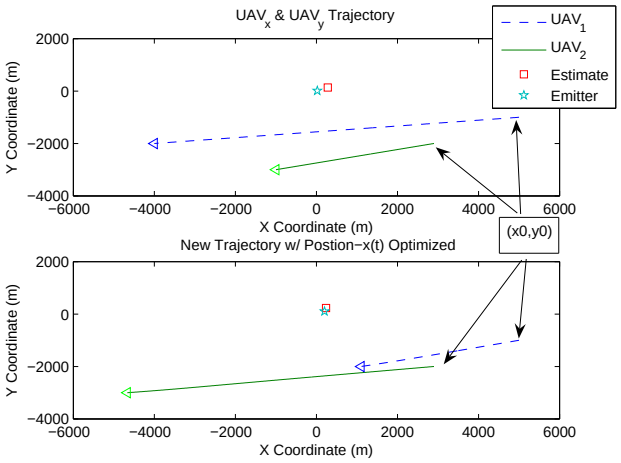

Figure 7: Velocity Control Simulation: UAV Trajectories

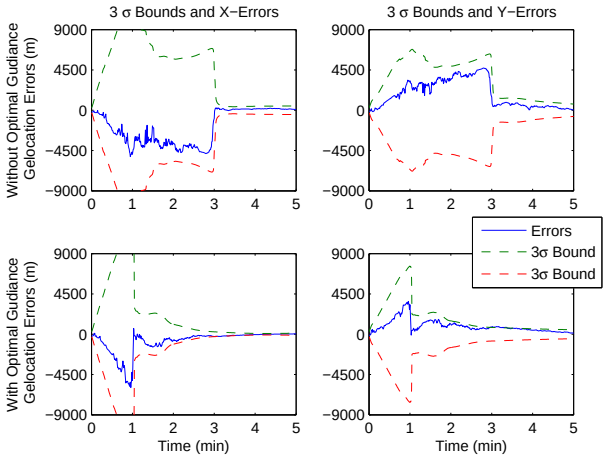

Figure 8: Velocity Control Simulation: Geolocation Errors and 3σ Bounds

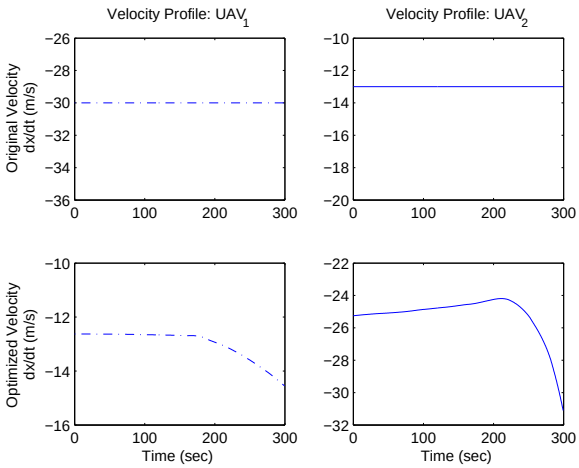

Figure 9: Velocity Control Simulation: $\dot{\mathbf{x}}_i(t)$ Control Input Profiles

ments in filter performance. Original UAV trajectories, 3σ bounds and velocities are seen in Figures 7, 8 and 9 (top plots) for the first routine using the EKF. The original linear paths give satisfactory observability between both UAVs and the EKF converges at $t \approx 3$ once the UAVs positions begin to separate from each other. This agrees with Section 5 investigations for cost function choice. By first manually increasing the geometric spacing of the UAVs the original filter converges.

Now, the stored EKF data is sent to the optimal guidance routine, then back to the EKF to estimate a new geolocation. In the bottom plots in Figures 7, 8 and 9 the guidance routine increases the separation between the two UAVs in order to maximize the $(H^T R^{-1} H)$ DOP quantity in Eqs. (19) and (20). Specifically the velocity control input to the UAV causes the separation distance to increase as seen in Figure 7. The weights on the control input are not equal to purposely aid in varying velocity control inputs. Yet, in Figure 9 the control inputs do not force improper motions but small variations to achieve quicker filter convergence. If the velocity differences are larger than a fewer meters per second then concern would be expressed for the UAV control system and structural components. The result on filter performance is lower geolocation error bounds for early segments of the simulation seen in Figure 8 and overall improved geolocation accuracy.

7 Conclusions

In this paper a suitable decentralized fusion architecture was described and developed for geolocation purposes. A hierarchical no-feedback decentralized architecture was selected as the best structure for a global geolocation. This structure

contains the simplest communication, team and team member requirements set forth, especially for UAVs. Then the CI algorithm proved useful to handle the sharing of redundant sensor information. For the two UAV case the CI provided fused information of equal or higher quality than each team individually.

In addition optimal control theory was applied to find improved UAV paths for enhance filter performance. In terms of geolocation a performance index was selected to minimize a particular DOP component of the error covariance of the KF update equation. The results in Section 6.2 showed that proper geometric space *before* and *after* running the guidance routine are necessary for the EKF to converge quicker. Also the routine eliminated the need to manually search for the proper velocity control inputs for each UAV. Last, geolocating for short periods of time allows for the propagation of co-states forward in time to find an acceptable minimum locally or globally based on the constraints to the system.

References

[1] Ho, K. C. and Chan, Y. C., "Solution and Performance Analysis of Geolocation by TDOA," *IEEE Transactions on Aerospace and Electronic Systems*, Vol. 29, No. 4, Oct 1993, pp. 1311–1322.

[2] Hall, D. L. and Llinas, J., *Handbook of Multisensor Data Fusion*, CRC Press,, Boca Raton, FL, 2001.

[3] Kayton, M., *Avionics Navigation Systems*, John Wiley & Sons, 1969, New York.

[4] Okello, N., "Emitter Geolocation with Multiple UAVs," *Proceedings of the* 9th *International Conference on Information Fusion*, July 2006.

[5] Chen, P., "A Cellular Based Mobile Location Tracking System," *IEEE* 49th *Vehicular Technology Conference*, Vol. 3, May 1999, pp. 1979–1983.

[6] Smith, J. O. and Abel, J. S., "Closed-Form Least-Squares Source Location Estimation from Range-Difference Measurements," *IEEE Transactions on Acoustics, Speech and Signal Processing*, Vol. 35, No. 12, Dec 1987, pp. 1661–1669.

[7] Schmidt, R., "Least Squares Range Difference Location," *IEEE Transactions on Aerospace and Electronic System*, Vol. 32, No. 1, Jan 1996, pp. 234–241.

[8] Savage, C. O., Cramer, R. L., and Schmitt, H. A., "TDOA Geolocation with the Unscented Kalman Filter," *Proceeding of the 2006 IEEE International Conference on Networking, Sensing and Control*, April 2006, pp. 602–606.

[9] Fletcher, F., Ristic, B., and Mušicki, D., "Recursive Estimation of Emitter Location using TDOA Measurements from Two UAVs," No. 1448, July 2007, pp. 1–8.

[10] Okello, D. M. N., "Emitter Geolocation with Two UAVs," *2007 Information Decision and Control*, Feb 2007, pp. 254–259.

[11] Okello, N. and Mušicki, D., "Measurement Association for Emitter Geolocation with Two UAVs," No. 1424, July 2007, pp. 1–8.

[12] Gao, Y., Krankiwsky, E., and Abousalem, M., "Comparison and Analysis of Centralized, Decentralized and Federated Filters," *Navigation: Journal of The Institute of Navigation*, Vol. 40, No. 1, Spring 1993, pp. 69–86.

[13] Liggins-II, M. E., Chong, C., Kadar, I., Alford, M. G., Vannicola, V., and Thomopoulos, S., "Distributed Fusion Architectures and Algorithms for Target Tracking," *Proceedings of the IEEE*, Vol. 85, No. 1, Janurary 1997, pp. 95–107.

[14] Schlosser, M. S. and Kroschel, K., "Communication Issues in Decentralized Kalman Filters," No. 3, June-July 2004.

[15] Reheeden, D. V., Brown, B., Price, J., Abbott, B., and Willden, G., "Automatic Positioning of UAVs to Optimize TDOA Geolocation Performance," *The* 23th *Digital Avionics Systems Conference., IEEE*, Vol. 2, Oct 2004, pp. 2.E.2–2.1–9.

[16] Crassidis, J. L. and Junkins, J. L., *Optimal Estimation of Dynamic Systems*, CRC Press, Boca Raton, FL, 2004.

[17] Julier, S. J. and Uhlmann, J. K., "A Non-divergent Estimation Algorithm in the Presence of Unknown Correlations," *Proceedings of the American Control Conference*, Vol. 4, No. 1234, June 1997, pp. 2369–2373.

[18] Lingji, C., Arambel, P. O., and Mehra, R. K., "Fusion under Unknown Correlation - Covariance Intersection as a Special Case," *Proceedings of the* 5th *International Conference on Information Fusion*, Vol. 2, July 2002, pp. 905–911.

[19] Rogers, R. M., *Applied Mathematics in Integrated Navigation Systems* 3th *Ed.*, American Institute of Aeronautics and Astronautics, Inc., Reston, VA, 2007.

[20] Kirk, D. E., *Optimal Control Theory, An Introduction*, Dover Publications, Inc., Mineola, NY, 1970.